lubricants

MDPI

Article

Scanning Electron Microscopy Texture Analysis of Brass, Aluminum and Mild Steel Worn Under Waste Cooking Oil Lubrication

Ayedh Eid Alajmi [1,*], Anthony Chukwunonso Opia [2,*], Kumaran Kadirgama [2], Jasem Alotaibi [1] and Belal F. Yousif [1,3,*]

[1] Department of Automotive and Marine Engineering Technology, Public Authority for Applied Education and Training, Adailiyah 42325, Kuwait; jg.alotaibi@paaet.edu.kw
[2] Centre for Sustainable Fluid Energy Research (Fluid Energy), Universiti Malaysia Pahang Al-Sultan Abdullah, Gambang 26300, Pahang, Malaysia; kumaran@umpsa.edu.my
[3] School of Engineering, University of Southern Queensland, Toowoomba, QLD 4350, Australia
* Correspondence: ae.alajmi@paaet.edu.kw (A.E.A.); anthony@umpsa.edu.my (A.C.O.); belal.yousif@unisq.edu.au (B.F.Y.)

Abstract

In bio-lubricant research, worn surfaces are usually interpreted qualitatively from scanning electron microscopy (SEM). This study tested how much tribological information objective, brightness-invariant texture descriptors can recover from an archive of such micrographs. Fifty-two ×1000 fields of brass, aluminum and mild steel worn against stainless steel at 40 N under fully synthetic oil and a 50/50 blend with waste cooking oil (WCO) at 22, 40 and 80 °C, plus four unworn references, were described by ten orientation, correlation-length, spectral and feature descriptors. Each condition is one specimen, so fields are repeated measurements; the analysis is descriptive at field level and inferential only at specimen level (13 specimens). Aluminum surfaces were less directional than brass and mild steel (orientation order 0.71 against 0.96 and 0.91), but a similar difference existed before wear, and at specimen level it was not significant ($p = 0.09$). Mild steel at 80 °C was strongly grooved (anisotropy 21 against 1.7 at 40 °C), with a fifteen-fold rise in measured roughness. Replacing half the synthetic oil with WCO left no detectable signature, and none of the 30 descriptor–response correlations were significant. Operator-selected single SEM fields document gross morphology but cannot rank lubricants or infer wear rate; an imaging protocol is proposed.

Keywords: bio lubricant; image analysis; worn surface; texture descriptors; structure tensor; lubricant temperature

Check for updates

Received: 20 October 2026
Revised: 6 November 2026
Accepted: 7 November 2026
Published: 16 November 2026

Copyright: © 2026 by the authors. Licensee MDPI, Basel, Switzerland. This article is an open access article distributed under the terms and conditions of the Creative Commons Attribution (CC BY) license.

1. Introduction

Bio lubricants derived from vegetable oils, and from waste cooking oil (WCO) in particular, are attractive replacements for mineral and synthetic base oils because they are renewable, biodegradable and, in the case of WCO [1,2], convert a waste stream into a product [3–5]. A body of work from this group has characterized WCO and its blends with a fully synthetic oil as lubricants for brass, aluminum and mild steel sliding against stainless steel, covering dry sliding [6,7], the effect of the WCO fraction, and the effect of lubricant temperature [8]. In those studies, as in most of the tribology literature, the worn surfaces were examined by scanning electron microscopy (SEM) and classified by eye into abrasive, adhesive, polishing and delamination features [8–10].

During tribological examinations, visual interpretation of micrographs has notable flaws if not thoroughly examined [11]. The operator selects the fields that are scanned, typically to highlight the most distinctive or striking aspects; the classification is based on experience; and the outcome is a label rather than a number that can be statistically linked to measured wear or compared between studies [11,12]. Quantitative descriptors of texture and orientation have been available for decades, from gray-level co-occurrence statistics and structure-tensor orientation analysis to spectral characterization of surface topography, and have been applied with success to wear particles [13,14]. Machine-learning analysis of tribological data is now growing rapidly [15]. What has not been established is whether the micrographs that tribology laboratories already hold, acquired for visual interpretation rather than for measurement, contain enough quantitative information to discriminate test conditions or to track measured wear.

Quantitative image analysis of worn surfaces has so far been applied mainly to engineered textures and wear particles rather than to the worn surfaces of lubricated metals. Ou et al. [16] performed a quantitative examination of the grinding performance of cubic silicon carbide surface texture lubricated with a water film, and found that micro-textured surfaces reduce friction, normal force, grinding temperature and subsurface damage relative to conventional surfaces, in agreement with earlier work [17,18]. Yu et al. [19] studied the effect of surface texture topography and orientation on point-contact mixed lubrication: isotropic bump arrays outperformed anisotropic arrangements because of efficient hydrodynamic pressure generation, and transverse grooves outperformed longitudinal grooves through lubricant trapping behind ridges, giving films up to 50% thicker. These studies show that the orientation and scale of surface texture govern film formation, which is the physical basis for expecting worn-surface texture to carry information about the lubricated contact. Lubricant selection and operating conditions, in particular temperature, also change the balance between fluid-film and boundary lubrication under severe operating conditions [20–22] which is the regime examined here.

The knowledge gap is therefore specific. The relation between a lubricant, its operating temperature and the resulting worn-surface texture of common engineering metals has been reported only qualitatively, and no study has asked whether the SEM archives that already exist can yield objective texture measures that separate test conditions. The hypothesis tested is that brightness-invariant descriptors of orientation, correlation length, spectral slope and feature content, computed on single ×1000 fields, differ between metals, lubricant temperatures and WCO fractions and co-vary with the measured specific wear rate, friction and roughness. This paper addresses that question directly using the complete ×1000 SEM archive from the WCO study of Alotaibi [2]. The aim was not to propose a new classifier but to determine, with conservative statistics, which tribological factors (metal, lubricant temperature, WCO fraction) leave a measurable signature in single-field SEM texture, whether those signatures relate to the measured specific wear rate, friction and roughness, and what the answer implies for how worn surfaces should be imaged in future bio-lubricant studies.

2. Materials and Methods

2.1. Tribological Tests and Measured Responses

The experimental program from the previous study [2] provides the micrographs and tribological data used in this investigation. Blocks of commercial brass, aluminum and mild steel were slid against a stainless-steel ring on a block-on-ring tribometer with a heated lubricant bath, at 40 N, 2.8 m/s and a sliding distance of 10.8 km. The lubricants were a fully synthetic oil (SO), WCO collected from local restaurants, and their blends; the WCO was modified with 5 wt.% ethylene vinyl acetate copolymer and 2 wt.% ethyl

cellulose to raise its viscosity [2]. Two blends tested at 40 N are represented in the SEM archive: 0% WCO (fully synthetic) and 50% WCO + 50% SO. Tests were run at lubricant temperatures of 22, 40 and 80 °C; the temperature series used the 50/50 blend. Each metal–blend–temperature condition was tested once, so the archive holds one specimen and one wear track per condition and a single value of each response. The specific wear rate, rate is the volume loss per unit load and sliding distance, $Ws = \Delta m/(\varrho\ F\ L)$, with Δm the mass loss, ϱ the metal density, F = 40 N and L = 10.8 km; it was recorded in the original workbook in $m^3\ N^{-1}\ m^{-1}$ and is reported here in $mm^3\ N^{-1}\ m^{-1}$. Lubricated values lie between 8×10^{-4} and 4 $mm^3\ N^{-1}\ m^{-1}$. The steady-state friction coefficient is the mean of the recorded friction force divided by the normal load over the final kilometer of sliding. The Ra was measured in the original experiments with a portable Mahr stylus surface roughness tester in accordance with ISO 4287, according to previous study [2], using a 0.8 mm cut-off and a 4 mm evaluation length, traversed perpendicular to the sliding direction at three locations within the central region of the wear track, with the reported value being the mean of these readings.

2.2. SEM Micrographs and Experimental Units

Worn and unworn surfaces were imaged [2] on a SEM, (JEOL-6000, JOEL Co., Tokyo, Japan) (magnifications of 200 nm) in high-vacuum secondary-electron mode at 10 or 15 kV. All fields recorded at ×1000 (1280 × 960 pixels, 0.0939 µm per pixel, field of view about 120 × 83 µm after removing the data bar) were included; ×1000 was the only magnification available for every condition. Table 1 lists the 52 worn and 4 unworn fields used in the analysis. The fields are repeated measurements on the same specimen: between one and seven fields (median four) were recorded per specimen, at positions chosen by the operator at the time of imaging to illustrate characteristic features, not sampled at random. The experimental unit for every inferential test in this paper is therefore the specimen, represented by the median of its fields; field-level statistics are reported as descriptive summaries of this archive only. The archive also holds ten fields of surfaces worn at 22 °C under pure WCO (five aluminum, three brass, one mild steel after a 100 N test, recorded under a nominal contact pressure of 226 kPa, and one aluminum field after a 50 N test, 113 kPa). These loads do not correspond to any row of the 40 N response table, so the ten fields were excluded from the condition matrix and from all comparisons.

Table 1. Number of ×1000 SEM fields per test condition (52 worn fields from 13 specimens, plus 4 unworn reference fields). Each non-zero cell is one specimen from one test run at 40 N, 2.8 m/s and 10.8 km against a stainless steel counterface.

Metal/Lubricant Temperature	Unworn	0% WCO (Fully Synthetic)	50% WCO + 50% SO
Brass, 22 °C	1	4	3
Brass, 40 °C		4	0
Brass, 80 °C		0	5
Aluminum, 22 °C	1	2	1
Aluminum, 40 °C		5	5
Aluminum, 80 °C		0	6
Mild steel, 22 °C	2	2	3
Mild steel, 40 °C		0	5
Mild steel, 80 °C		0	7

WCO: waste cooking oil; SO: fully synthetic oil. Ten further fields worn under pure WCO at 100 N and 50 N are excluded (Section 2.2).

2.3. Image Descriptors

As brightness and contrast settings differed between imaging sessions, every descriptor was computed on a normalized image. The data bar was removed by cropping to the top 880 rows. The slowly varying illumination was removed by subtracting a Gaussian-smoothed copy (σ = 60 pixels, reflective boundaries); the residual was converted to a z-score, and the z-score over the field was computed; detector noise below 0.25 µm was suppressed by a Gaussian filter of σ = 0.25 µm (2.7 pixels) and the result was re-standardized. Ten descriptors were then computed (Table 2). Gradients for the structure tensor were obtained with 3 × 3 Sobel operators applied after a 1-pixel Gaussian pre-smoothing; the tensor components were integrated with a Gaussian window of σ = 1.5 µm. Orientation order R is the modulus of the mean of $\exp(2i\theta)$ over the field weighted by the tensor trace, and coherence is the trace-weighted mean of $(\lambda_1 - \lambda_2)/(\lambda_1 + \lambda_2)$. The two-dimensional autocorrelation was computed through the Fourier transform (circular boundary) and normalized to unity at zero lag; the correlation length along and across the dominant orientation is the first lag at which the autocorrelation falls below 1/e, sampled by linear interpolation at 1-pixel steps up to 300 pixels (28.2 µm). Where the autocorrelation had not fallen to 1/e within 28.2 µm, the length was recorded as 28.2 µm, a censored value; this occurred for the along-groove length in 14 of the 52 worn fields, all strongly grooved, so anisotropy is a lower bound for those fields. The spectral exponent β is the negative slope of a least-squares line through the log radially averaged power spectrum of the Hann-windowed field between wavelengths of 2 and 20 µm. The feature mask is the set of pixels whose magnitude exceeds 2.5 standard deviations after Gaussian smoothing at 0.5 µm and re-standardization, followed by one binary opening with a 3 × 3 cross structuring element; the feature area fraction is its area fraction and the feature density is the number of connected components (8-connectivity) per 1000 µm^2. For the gray-level co-occurrence matrix, the normalized image was clipped to ±3 and mapped linearly to 32 gray levels, and the symmetric normalized matrix was computed at an offset of 1 µm (11 pixels) in four directions; homogeneity and contrast are the means over directions. Figure 1 illustrates the main steps on one micrograph, and the complete Python 3.10.7 implementation.

Table 2. The ten image descriptors computed on each illumination-corrected, contrast-normalized micrograph.

s/*n*	Descriptor	Definition	Physical Reading
1.	Groove orientation order, R	Modulus of the trace-weighted mean of $\exp(2i\theta)$ over the structure-tensor orientation field (0 = isotropic, 1 = all features parallel)	Directionality of linear features across the field
2.	Local coherence	Trace-weighted mean of $(\lambda_1 - \lambda_2)/(\lambda_1 + \lambda_2)$ of the structure tensor at 1.5 µm integration scale	Local line-likeness of the texture
3.	Correlation length across grooves (µm)	First lag at which the normalized 2D autocorrelation falls below 1/e, measured perpendicular to the dominant orientation	Width scale of grooves and ridges
4.	Correlation length along grooves (µm)	As above, measured parallel to the dominant orientation (censored at 28.2 µm)	Continuity of grooves
5.	Anisotropy	Ratio of a long-groove to a cross-groove correlation length	Elongation of surface features
6.	Spectral exponent, β	Negative slope of the radially averaged power spectrum between 2 and 20 µm wavelengths	Balance of coarse to fine texture (higher β = smoother at fine scale)

Table 2. *Cont.*

s/*n*	Descriptor	Definition	Physical Reading
7.	Feature area fraction (%)	Area fraction of the feature mask ($\|z\| > 2.5$ SD after 0.5 µm smoothing, one binary opening)	Area of high-contrast features: pits, flakes, debris, groove edges
8.	Feature density (per 1000 µm^2)	Number of connected components of the feature mask per 1000 µm^2	Fragmentation of high-contrast features
9.	GLCM homogeneity	Mean over four directions of $\Sigma\, p(i,j)/(1 + \|i - j\|)$ at 1 µm offset, 32 levels	Fine-scale regularity
10.	GLCM contrast	Mean over four directions of $\Sigma\, (i - j)^2\, p(i,j)$ at 1 µm offset, 32 levels	Fine-scale local variation

All descriptors are computed on the z-scored image and are therefore invariant to the absolute brightness and to a linear change in contrast of the SEM, which varied between imaging sessions; they are not invariant to accelerating voltage, which is treated as a confounder in Section 2.4.

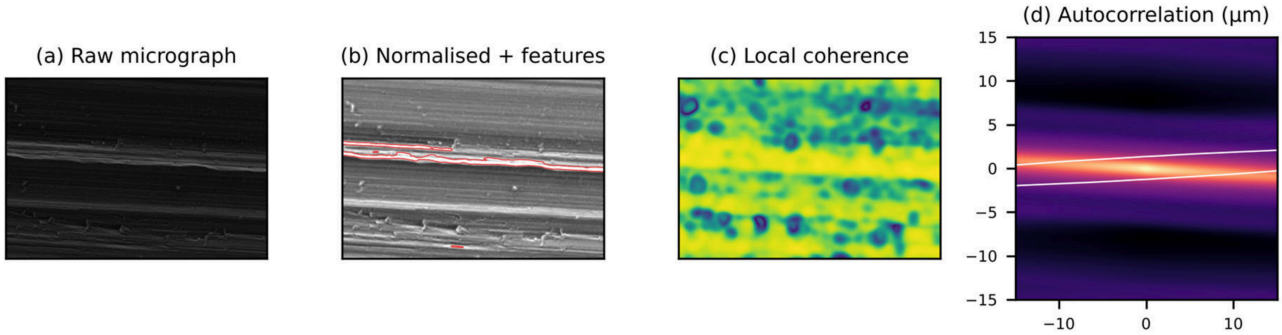


Figure 1. Image processing applied to a mild steel field (80 °C, 50% WCO): (**a**) raw micrograph; (**b**) illumination-corrected, normalized image with detected features outlined; (**c**) local structure-tensor coherence; (**d**) central region of the autocorrelation with the 1/e contour, showing elongation along the sliding direction.

2.4. Statistics

The analysis is exploratory and is reported as such. Because each condition is a single specimen, differences between metals were tested with the Kruskal–Wallis test on the specimen-level medians (4 brass, 5 aluminum and 4 mild steel specimens), and lubricant and temperature effects, which compare single specimens, are reported descriptively with the spread of fields shown as interquartile ranges. Field-level Kruskal–Wallis and Mann–Whitney tests, in which fields are treated as replicates, are reported only as descriptive summaries of this archive. Because the accelerating voltage changed between sessions and is partly confounded with condition, every field-level contrast was also examined within a single voltage. Relationships with the measured responses were tested by Spearman rank correlation between the specimen-level descriptor medians and the recorded specific wear rate ($\log_{10}$), friction coefficient and Ra over the 13 conditions; 95% confidence intervals were obtained by bootstrap (5000 resamples of the 13 conditions). A within-metal version ranked descriptor and response separately inside each metal (average ranks for ties; group sizes 4, 5 and 4) and pooled the ranks. Three families of comparisons were defined: the 10 metal tests, the 10 temperature tests per metal and the 30 correlations, and Holm-adjusted *p*-values are reported within each family. The sensitivity of the two headline results to the processing parameters (illumination σ, noise filter, tensor integration scale, feature threshold and smoothing, GLCM offset, morphological opening) was examined by recomputing all descriptors over a range of each parameter (Section 3.6).

3. Results

3.1. Qualitative Appearance

Representative fields are shown in Figure 2, chosen as the field closest to the condition median of orientation order. Unworn brass and mild steel carry fine parallel machining marks, and unworn aluminum a coarser, torn finishing texture. After lubricated sliding at 22 °C, all three metals show smoothed surfaces with shallow grooves parallel to the sliding direction, consistent with the polishing and mild abrasion described in [2,23]. At 80 °C, the aluminum surface carries wide, deep grooves with folded and smeared material at their edges, and the mild steel surface is covered by continuous parallel grooves, whereas brass remains comparatively smooth, thus similar to previously conducted studies [24–26].

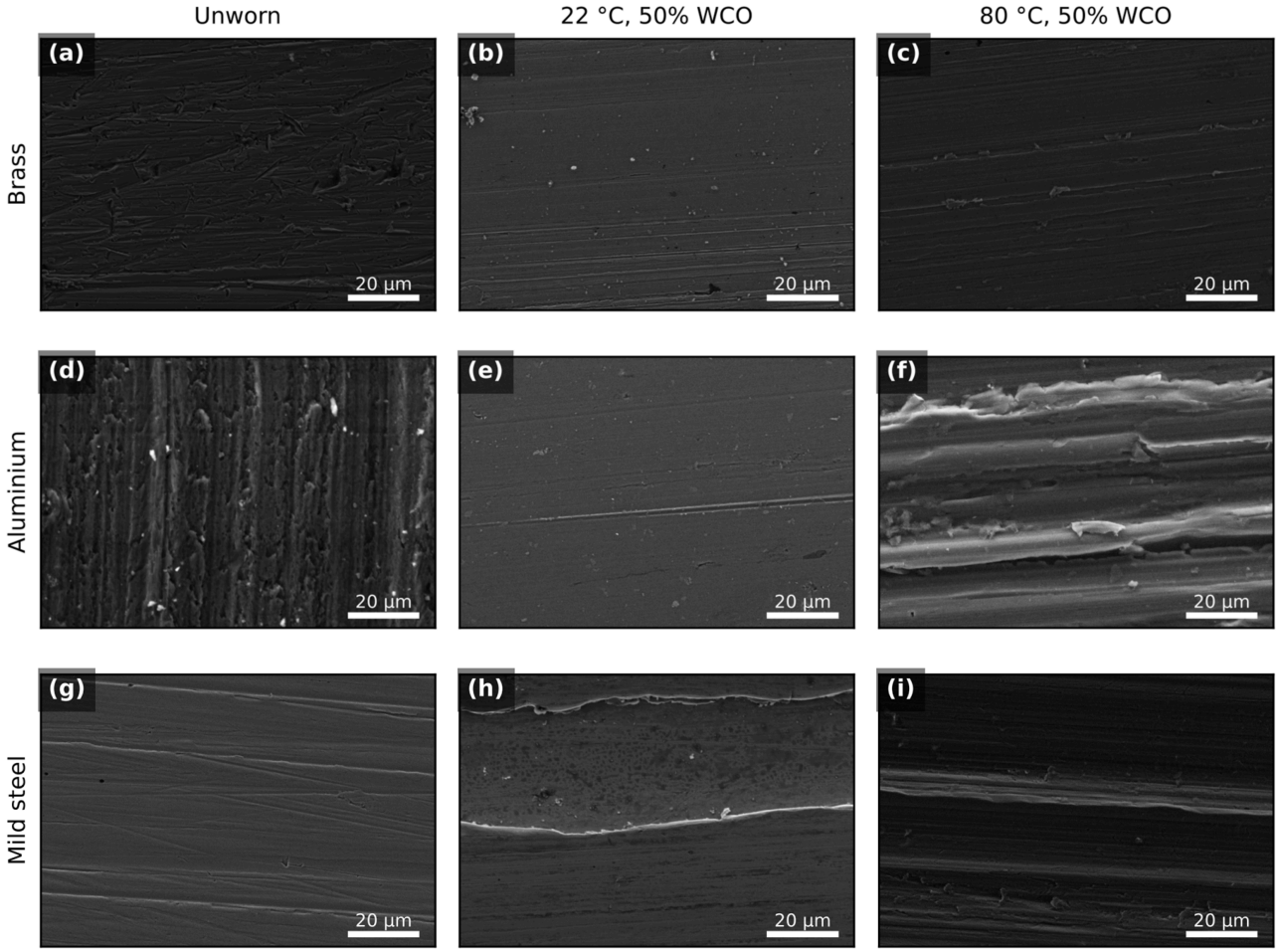


Figure 2. Representative ×1000 SEM fields of brass (**a**–**c**), aluminum (**d**–**f**) and mild steel (**g**–**i**): unworn (**left**), after sliding at 22 °C with 50% WCO (**center**) and at 80 °C with 50% WCO (**right**). Sliding direction is horizontal.

3.2. Differences Between Metals and the Unworn Baseline

Table 3 gives all ten descriptors by metal at both levels, and Figure 3 shows the four most informative. Over the worn fields, aluminum was the least directional surface: its median orientation order was 0.706 against 0.95 for brass and 0.911 for mild steel, its median anisotropy was 2.3 against 26 and 11, and it had the widest across-groove correlation length (1.13 µm) while brass had the narrowest (0.56 µm). Aluminum also had the highest feature area fraction (3.3%). At the specimen level, which is the valid unit, the same ordering is present (orientation order 0.71, 0.96 and 0.91) but with 4, 5 and 4 specimens the Kruskal–Wallis test gives $p = 0.094$ for orientation order and p between 0.043 (GLCM contrast) and

0.85 for the other descriptors, and no descriptor is significant after Holm adjustment. The metal contrast is therefore a consistent and large descriptive difference in this archive rather than a statistically established effect.

Table 3. All ten descriptors by metal. Field-level values are medians [interquartile range] over all worn fields and are descriptive. Specimen-level values are the median of the 4, 5 and 4 condition medians per metal; p is the Kruskal–Wallis test on these specimen-level values (the experimental unit), with Holm adjustment over the ten descriptors.

Descriptor	Brass Fields (n = 16)	Aluminum Fields (n = 19)	Mild Steel Fields (n = 17)	Brass Spec. (n = 4)	Al Spec. (n = 5)	Steel Spec. (n = 4)	p (Spec.)	p Holm
Groove orientation order, R	0.95 [0.887–0.977]	0.706 [0.593–0.869]	0.911 [0.838–0.937]	0.957	0.706	0.905	0.094	0.730
Local coherence	0.718 [0.672–0.753]	0.527 [0.418–0.678]	0.711 [0.398–0.849]	0.71	0.477	0.683	0.472	1.000
Anisotropy	26.2 [9.09–36.2]	2.33 [1.58–13.7]	11.4 [1.78–21.4]	26.9	2.33	10.8	0.225	0.898
Correlation length across grooves (µm)	0.563 [0.563–0.587]	1.13 [0.845–1.36]	0.939 [0.751–1.22]	0.563	0.986	0.822	0.091	0.730
Correlation length along grooves (µm)	14.7 [5.28–27.1]	2.63 [1.97–20.7]	10.7 [1.6–28.2]	16.6	2.3	10.4	0.849	1.000
Spectral exponent, β	1.38 [1.25–1.75]	2.51 [1.93–2.67]	2.61 [1.79–2.74]	1.52	1.84	2.17	0.103	0.730
Feature area fraction (%)	2.36 [1.7–2.6]	3.3 [2.53–3.66]	3 [2.33–3.45]	2.04	2.59	3.14	0.131	0.730
Feature density (per 1000 µm^2)	7.3 [5.56–8.38]	5.44 [4.23–6.75]	2.62 [1.91–7.25]	7.28	5.54	5.84	0.511	1.000
GLCM homogeneity	0.267 [0.237–0.296]	0.452 [0.335–0.492]	0.334 [0.296–0.449]	0.267	0.438	0.353	0.081	0.730
GLCM contrast	32.1 [28.9–40.2]	19 [15.4–24.2]	22.8 [14.6–30.9]	33.7	19.7	25.2	0.043	0.426

Field-level Kruskal–Wallis p-values, which treat fields as independent, are below 0.01 for seven of the ten descriptors; they are not used for inference because fields from one specimen are not independent replicates.

Table 4 shows why the directional contrast must be read with care. The unworn aluminum reference already has a low orientation order (0.72) and a short along-groove correlation length (2.2 µm), while unworn brass (0.91) and especially unworn mild steel (0.98) carry strongly directional machining marks. Wear raised the orientation order of brass slightly (0.91 to 0.96), lowered that of mild steel (0.98 to 0.91) and left that of aluminum essentially unchanged (0.72 to 0.71). The lower directionality of worn aluminum is thus largely inherited from its finishing texture, and the descriptors measure surface morphology, not wear mechanism. What did change clearly with wear is the feature content: the feature area fraction of aluminum rose from 1.7% to 2.6%, and its feature density fell, consistent with the replacement of fine finishing marks by larger pits, flakes and adhered debris, and the spectral exponent of brass rose from 1.0 to 1.5 as fine-scale machining texture was polished away. The fields imaged at 10 kV and at 15 kV showed the same ordering of metals in orientation order (descriptive), so the contrast is not an artifact of accelerating voltage. In the matched conditions in which all three metals were imaged, the ordering aluminum < brass ≈ steel holds at 22 °C under synthetic oil (0.61, 0.97, 0.88) but not at 80 °C with 50% WCO (0.93, 0.94, 0.97), where all three metals are strongly grooved. The ordering

agrees with the measured wear: aluminum had specific wear rates between one and more than two orders of magnitude higher than brass and mild steel at every condition [2,27–29].

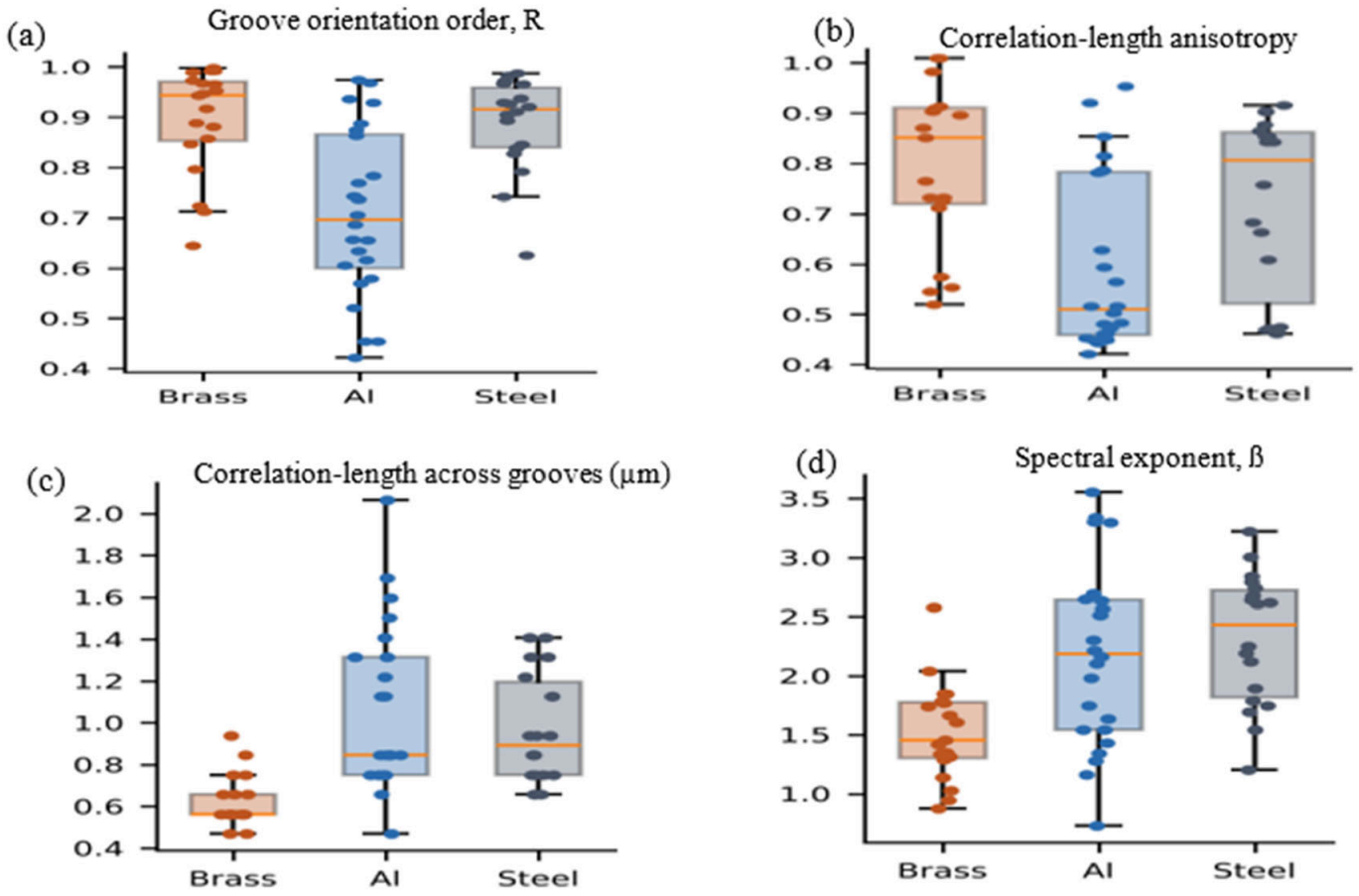


Figure 3. Distribution of four descriptors over all worn fields for each metal. Boxes show the interquartile range and median of the fields; small points are individual fields; diamonds are the specimen-level medians used for inference. Under grove orientation order, brass and steel had similar trend with higher wear compared to aluminum as shown in (**a**). For correlation-length anisotropy, brass demonstrates higher value followed by steel before aluminum as presented in (**b**). Investigating correlation length across groves, brass revealed the least value, while steel and aluminum yielded similar results as demonstrates in (**c**), thus similar outcome was discovered under spectral exponent as depicts in (**d**).

Table 4. Descriptors of the unworn reference surfaces (number of fields in brackets; steel is the median of two) beside the specimen-level worn median for the same metal.

Descriptor	Brass Unworn (1)	Brass Worn	Al Unworn (1)	Al Worn	Steel Unworn (2)	Steel Worn
Groove orientation order, R	0.906	0.957	0.723	0.706	0.984	0.905
Local coherence	0.698	0.71	0.435	0.477	0.905	0.683
Anisotropy	5.33	26.9	2.3	2.33	33.4	10.8
Corr. length across grooves (µm)	0.563	0.563	0.939	0.986	0.657	0.822
Corr. length along grooves (µm)	3	16.6	2.16	2.3	21.9	10.4

Table 4. *Cont.*

Descriptor	Brass Unworn (1)	Brass Worn	Al Unworn (1)	Al Worn	Steel Unworn (2)	Steel Worn
Spectral exponent, β	1	1.52	1.64	1.84	1.71	2.17
Feature area fraction (%)	2.89	2.04	1.74	2.59	3.37	3.14
Feature density (per 1000 μm^2)	10.5	7.28	6.34	5.54	3.57	5.84
GLCM homogeneity	0.255	0.267	0.289	0.438	0.329	0.353
GLCM contrast	42.1	33.7	22.2	19.7	29.9	25.2

3.3. Effect of Lubricant Temperature

Figure 4 shows orientation order and anisotropy against lubricant temperature for the 50/50 blend; each temperature is one specimen, so the comparison is descriptive. Mild steel showed the clearest change: the surface at 80 °C was strongly grooved (median anisotropy 21, orientation order 0.97) compared with 40 °C (1.7 and 0.79). The spread of fields within each specimen was small relative to this difference: the interquartile ranges of anisotropy at 40 and 80 °C (1.7–1.8 and 21–26) do not overlap, and the same separation holds when only the 15 kV fields are compared ($n = 3$ and 7). Among the ten descriptors, the three-temperature field-level Kruskal–Wallis test for mild steel gave $p \leq 0.05$ for nine, of which five remain below 0.05 after Holm adjustment within that family; given one specimen per temperature, these values describe the consistency of the fields, not independent replication. The change coincided with the largest change in the measured data: the Ra of mild steel rose from 0.24 μm at 40 °C to 2.8 μm at 80 °C, and its friction coefficient rose from 0.043 to 0.115. Brass also became more directional between 22 and 80 °C (orientation order 0.72 to 0.94, field-level $p = 0.025$, not significant after Holm adjustment). For aluminum, the 40 °C fields were the least ordered of any condition, but the single 22 °C field prevents a firm conclusion. The non-monotonic pattern for steel and aluminum, with the least ordered surfaces at 40 °C, has no counterpart in the measured wear, which rose steadily with temperature for every metal.

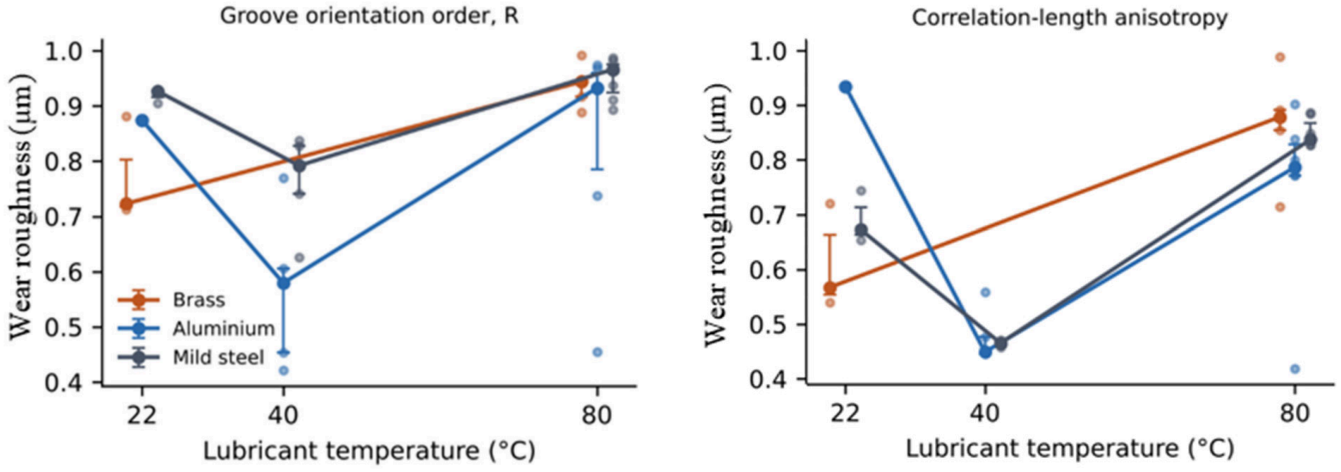


Figure 4. Orientation order and anisotropy against lubricant temperature for the 50% WCO blend. Small points are individual fields; markers and bars are the specimen median and interquartile range. Brass was not imaged at 40 °C with this blend.

3.4. Effect of WCO Fraction

Because the metal effect is large, lubricant comparisons were made within each metal (Table 5). Only the fully synthetic oil and the 50/50 blend were imaged at 40 N; the pure-WCO images in the archive come from 100 N and 50 N tests and were excluded (Section 2.2), so the original pooled comparison of three blends across metals has been withdrawn. At 22 °C, each blend is a single specimen with one to five fields, so no inferential test was applied. For brass, the only metal with at least three fields for both blends, the fully synthetic oil gave the more directional surface (orientation order 0.97, anisotropy 25) and the 50/50 blend the less directional (0.72, 3.4; descriptive Mann–Whitney $p = 0.11$), while the across-groove length, spectral exponent and feature fraction did not differ. For aluminum (two and one fields) and mild steel (two and three fields), the data are insufficient for any statement. At 40 °C, aluminum was imaged under both blends with five fields each; the 50/50 blend gave a less directional surface (orientation order 0.58 against 0.71) with a wider across-groove length (1.3 against 0.8 µm), again a single-specimen difference. The available data are therefore insufficient to establish or exclude an effect of WCO fraction on worn-surface texture; what can be said is that no difference between the two blends approaches the size of the difference between metals or between 40 and 80 °C, which is consistent with the measured data, in which replacing half the synthetic oil with WCO changed the specific wear rate of each metal by less than a factor of four and Ra by less than 0.06 µm at room temperature [2,30–32].

Table 5. Lubricant comparison at 22 °C and 40 N stratified by metal: median of the fields for each blend (number of fields in brackets). Each cell is one specimen. The pure WCO images at 22 °C were recorded after a 100 N test and are not part of this comparison.

Metal	Descriptor	0% WCO (SO)	50% WCO
Brass	Groove orientation order, R	0.969 ($n = 4$)	0.723 ($n = 3$)
Brass	Anisotropy	25.5 ($n = 4$)	3.43 ($n = 3$)
Brass	Correlation length across grooves (µm)	0.657 ($n = 4$)	0.563 ($n = 3$)
Brass	Spectral exponent, β	1.7 ($n = 4$)	1.78 ($n = 3$)
Brass	Feature area fraction (%)	2.61 ($n = 4$)	1.74 ($n = 3$)
Aluminum	Groove orientation order, R	0.613 ($n = 2$)	0.874 ($n = 1$)
Aluminum	Anisotropy	2.33 ($n = 2$)	41.4 ($n = 1$)
Aluminum	Correlation length across grooves (µm)	0.986 ($n = 2$)	0.469 ($n = 1$)
Aluminum	Spectral exponent, β	1.84 ($n = 2$)	0.729 ($n = 1$)
Aluminum	Feature area fraction (%)	2.46 ($n = 2$)	2.59 ($n = 1$)
Mild steel	Groove orientation order, R	0.883 ($n = 2$)	0.926 ($n = 3$)
Mild steel	Anisotropy	14.6 ($n = 2$)	7 ($n = 3$)
Mild steel	Correlation length across grooves (µm)	0.892 ($n = 2$)	0.751 ($n = 3$)
Mild steel	Spectral exponent, β	2.21 ($n = 2$)	2.12 ($n = 3$)
Mild steel	Feature area fraction (%)	3.67 ($n = 2$)	3.23 ($n = 3$)

3.5. Relationship with Measured Wear, Friction and Roughness

None of the 30 correlations between a specimen-level descriptor and a measured response was significant (Table 6; unadjusted $p \geq 0.066$, Holm-adjusted $p \geq 0.66$). The strongest associations were negative correlations of GLCM contrast with log specific wear rate ($\varrho = -0.51$, 95% CI −0.85 to 0.06, $p = 0.074$) and with Ra ($\varrho = -0.52$, $p = 0.066$), and of

orientation order with log specific wear rate ($\varrho = -0.42$, 95% CI −0.80 to 0.13, $p = 0.15$); all are driven by the metal effect in Section 3.2, since brass has both the highest GLCM contrast and the lowest wear, and once the variables were ranked within each metal they fell to $|\varrho| \leq 0.36$. Figure 5 shows the reason. Conditions with very different wear rates, for example aluminum at 22 °C and at 80 °C, which differ by a factor of about 80, can have similar orientation order, while conditions with similar wear can lie at opposite ends of the descriptor range. The absence of correlation reflects both a measurement mismatch, since the responses are whole-track averages while each descriptor summarizes about 0.01 mm^2 of operator-selected surface, and the small number of specimens, which gives the correlations wide confidence intervals: with 13 conditions only $|\varrho|$ above about 0.55 could have been detected.

Table 6. Spearman rank correlation between the specimen-level descriptor and the measured specific wear rate (SWR), friction coefficient (μ) and worn-surface roughness (Ra) over the 13 test conditions at 40 N, with bootstrap 95% confidence intervals (5000 resamples) for log SWR.

Descriptor (Specimen Median)	log SWR, ϱ [95% CI]	μ, ϱ	Ra, ϱ	Log SWR Within-Metal ϱ	Holm p (log SWR)
Groove orientation order, R	−0.42 [−0.80, 0.13]	0.26	−0.12	0.29	1.000
Local coherence	−0.20 [−0.66, 0.35]	0.31	0.12	0.28	1.000
Anisotropy	−0.14 [−0.63, 0.39]	0.18	0.03	0.24	1.000
Correlation length across grooves (μm)	0.42 [−0.25, 0.86]	0.27	0.43	0.22	1.000
Correlation length along grooves (μm)	0.02 [−0.62, 0.62]	0.32	0.25	0.28	1.000
Spectral exponent, β	0.26 [−0.43, 0.76]	0.29	0.36	0.17	1.000
Feature area fraction (%)	0.21 [−0.43, 0.85]	0.08	0.19	0.15	1.000
Feature density (per 1000 μm^2)	−0.16 [−0.69, 0.53]	−0.15	−0.41	−0.35	1.000
GLCM homogeneity	0.36 [−0.22, 0.78]	−0.06	0.31	−0.14	1.000
GLCM contrast	−0.51 [−0.85, 0.06]	−0.15	−0.52	−0.18	0.743

Within-metal ϱ: descriptor and response were ranked separately inside each metal (groups of 4, 5 and 4 conditions, average ranks for ties) and the ranks pooled, which removes the offset in wear rate between metals.

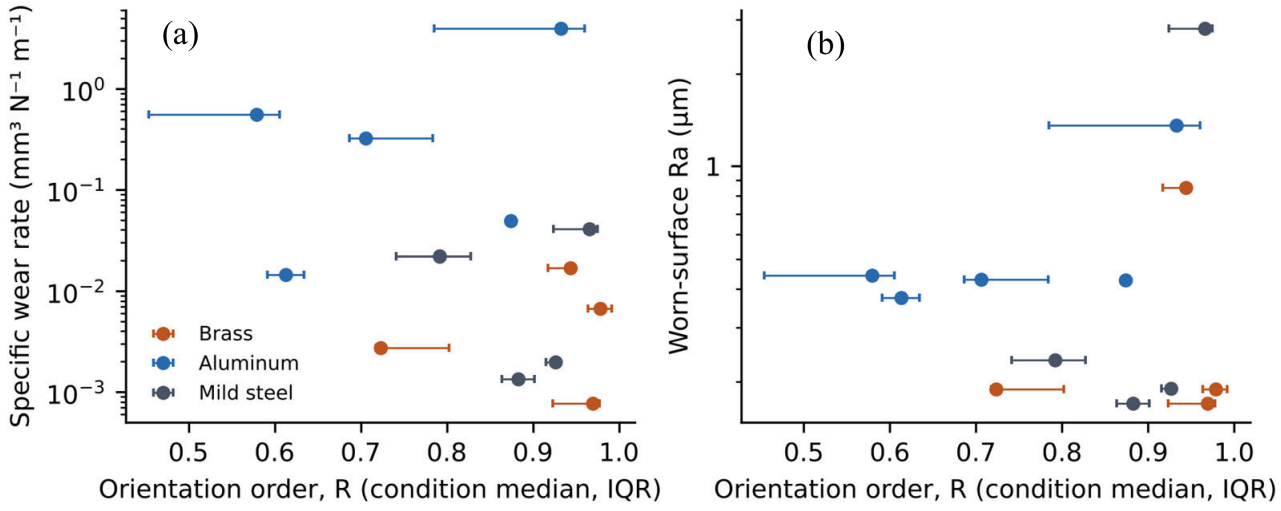


Figure 5. Specimen-level orientation order (median, bars = interquartile range of the fields) against (**a**) the specific wear rate (mm^3 N^{-1} m^{-1}) and (**b**) worn-surface Ra for the 13 metal, blend and temperature conditions at 40 N.

3.6. What the Descriptors Respond to, and Their Sensitivity to Processing Choices

Figure 6 shows the feature mask and orientation field on four annotated examples. On unworn brass (Figure 6a), the mask selects the edges of machining marks, and the high orientation order reflects those marks, not wear. On aluminum at 80 °C (Figure 6b), the mask selects the bright lips of deep grooves and smeared material, and on aluminum at 40 °C under the 50/50 blend (Figure 6c), it selects pits and adhered debris; the two give similar feature fractions (3.1% and 3.7%), although the morphology is different. On mild steel at 80 °C (Figure 6d), the mask selects groove edges, and the orientation order is 0.97. The feature fraction therefore measures the area of high-contrast features of any kind, and the orientation descriptors measure directionality of any origin; neither identifies a wear mechanism on its own, and the interpretation in Section 4 is restricted accordingly.

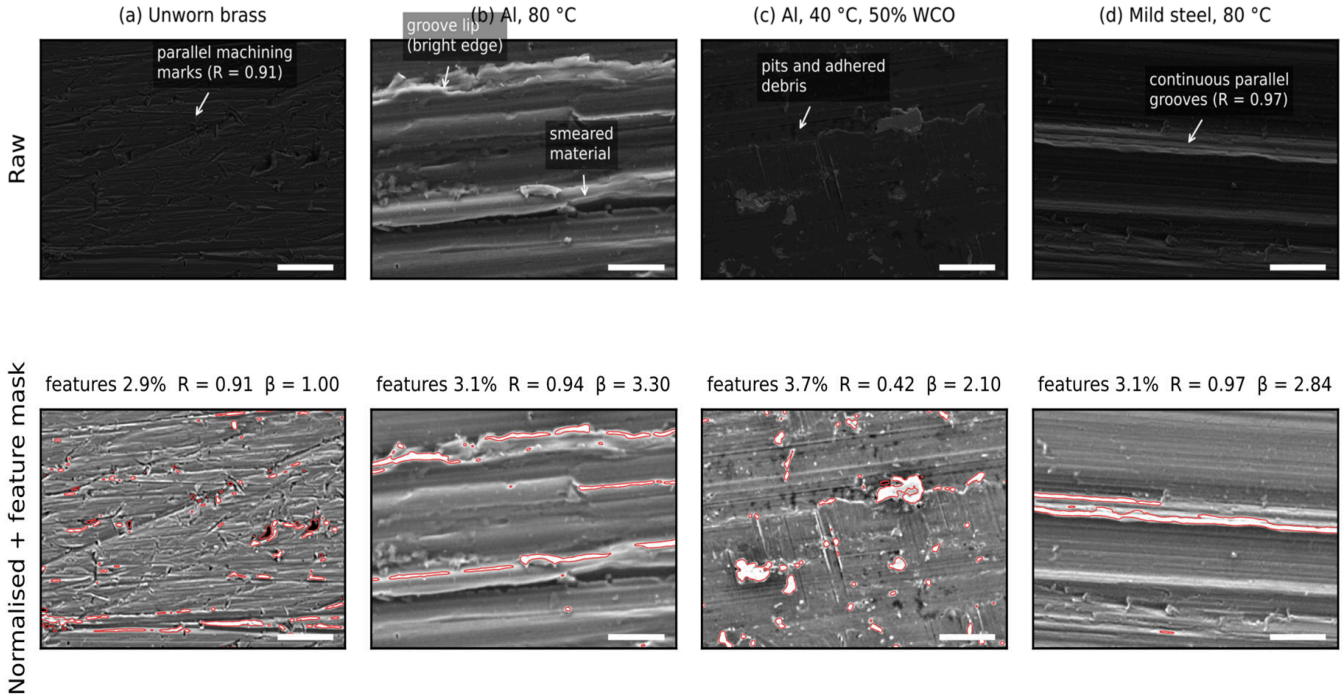


Figure 6. Annotated examples of what the descriptors respond to. Top: raw fields of (**a**) unworn brass, (**b**) aluminum at 80 °C with 50% WCO, (**c**) aluminum at 40 °C with 50% WCO and (**d**) mild steel at 80 °C with 50% WCO. Bottom: the normalized image with the feature mask outlined in red and the field's feature fraction, orientation order and spectral exponent. Scale bars: 20 µm; sliding direction horizontal.

Table 7 shows that the two headline comparisons do not depend on the processing parameters. Across changes in the illumination scale (40–80 pixels), the noise filter (0.15–0.35 µm), the structure-tensor integration scale (1.0–2.0 µm), the feature threshold (2.0–3.0 SD) and smoothing (0.35–0.75 µm), the GLCM offset (0.5–2.0 µm) and removal of the morphological opening, the median orientation order of aluminum stayed below that of brass and mild steel by 0.18 to 0.26, the specimen-level Kruskal–Wallis p for orientation order stayed between 0.06 and 0.13, and the mild steel anisotropy at 80 °C stayed more than ten times that at 40 °C. The GLCM offset changes the absolute values of homogeneity and contrast but not the ordering of the metals. The tensor integration scale shifts the absolute orientation order of all metals together, by about 0.05 per 0.5 µm, so values of R are comparable only at a stated scale.

Table 7. Sensitivity of the two headline comparisons to the processing parameters. R: median orientation order over worn fields. p metal: Kruskal–Wallis on specimen-level medians. The steel comparison is the field-level Mann–Whitney test at 15 kV ($n = 3$ and 7), reported for comparability with the original submission.

Setting	R Al	R Brass	R Steel	p Metal (Specimen)	Steel Anisotropy 40/80 °C	p Steel 40 vs. 80 °C (15 kV)
Baseline	0.706	0.95	0.911	0.0941	1.71/21.43	0.0218
Illumination $\sigma = 40$ px	0.706	0.95	0.91	0.0941	1.86/25.0	0.0222
Illumination $\sigma = 80$ px	0.706	0.95	0.911	0.0941	1.71/18.75	0.021
Noise filter 0.15 µm	0.729	0.961	0.92	0.0555	1.8/23.08	0.021
Noise filter 0.35 µm	0.67	0.946	0.911	0.1336	1.78/20.0	0.0218
Tensor scale 1.0 µm	0.618	0.927	0.875	0.0941	1.71/21.43	0.0218
Tensor scale 2.0 µm	0.759	0.962	0.935	0.0941	1.71/21.43	0.0218
Feature threshold 2.0 SD	0.706	0.95	0.911	0.0941	1.71/21.43	0.0218
Feature threshold 3.0 SD	0.706	0.95	0.911	0.0941	1.71/21.43	0.0218
Feature smoothing 0.35 µm	0.706	0.95	0.911	0.0941	1.71/21.43	0.0218
Feature smoothing 0.75 µm	0.706	0.95	0.911	0.0941	1.71/21.43	0.0218
GLCM offset 0.5 µm	0.706	0.95	0.911	0.0941	1.71/21.43	0.0218
GLCM offset 2.0 µm	0.706	0.95	0.911	0.0941	1.71/21.43	0.0218
No morphological opening	0.706	0.95	0.911	0.0941	1.71/21.43	0.0218

4. Discussion

The analysis shows that the SEM archive contains consistent information about worn-surface morphology but, with one specimen per condition, cannot by itself establish effects of metal or lubricant, and contains no detectable information about wear amount. The material contrast, aluminum surfaces being less directional and more pitted than brass and mild steel, is large and consistent across imaging voltages and agrees with the visual classification of aluminum as the metal most affected by adhesion, plowing and material transfer under these lubricants [2,22,33–36]. Its directional component, however, was already present before wear (Table 4), so the descriptors that separate the metals most clearly are measuring finishing texture as much as wear; the feature content and spectral slope, which did change with wear, are the better indicators of wear morphology in this archive. The thermally induced transition of mild steel to a deeply grooved surface at 80 °C is recovered by the descriptors and coincides with the jump in measured roughness and friction, which supports the interpretation that thinning of the lubricant film at high temperature allowed asperity contact and abrasion by the harder counter face [2], although with one specimen per temperature this remains an observation to be tested by replication.

Three factors explain why the same descriptors do not track specific wear rate. First, morphology and wear volume are different quantities: a polished surface and a uniformly grooved one can lose material at very different rates while presenting similarly ordered textures, a point implicit in Archard-type wear relations, where volume depends on load, distance and hardness rather than on surface pattern [7]. Second, a ×1000 field covers about 0.01 mm^2 of a wear track several square millimeters in area, and the fields in this archive were chosen by the operator to illustrate features rather than sampled at random. Third, imaging conditions were not standardized; although brightness-invariant descriptors and within-voltage checks control for the most obvious bias, the accelerating voltage changes the depth of information in secondary-electron images and cannot be fully separated from test conditions in this archive.

These findings have a practical consequence for bio lubricant research, where SEM is often used as the main evidence that one blend protects a surface better than another. In

the present data, replacing half the synthetic oil with WCO fraction left no measurable trace in the surface texture within any metal, in agreement with its small effect on measured wear. Claims that a lubricant changes the wear mechanism should therefore be supported by quantitative descriptors computed on systematically sampled fields, not by selected micrographs alone. A protocol that would make such claims testable is: (i) fix accelerating voltage, working distance, detector and magnification for a whole study; (ii) test at least three independent specimens per condition and image at least five fields per specimen at predefined positions along and across the wear track; (iii) record and archive the raw images with their metadata; (iv) report orientation, correlation-length and spectral descriptors alongside wear and roughness, together with the same descriptors of the unworn surface; and (v) pair SEM with an areal topography measurement where wear-volume inferences are made. The protocol has not yet been validated; its validation on a replicated test series is the subject of a following study.

The study has limitations. Each condition is a single specimen, so between-condition comparisons are descriptive; the number of fields per specimen is small and unequal; several conditions are represented by one or two fields; and the significance thresholds, where quoted, are exploratory and reported with Holm adjustment within defined families. The tribological responses are single values per condition taken from the original data set, so their own uncertainty could not be propagated. The pure-WCO surfaces in the archive were worn at other loads and could not be included, so the comparison of blends is limited to the 50/50 blend against synthetic oil. The descriptors are deliberately simple and interpretable; more complex learned features might extract more information, but on an archive of this size they would be at high risk of overfitting.

5. Conclusions

Fifty-two archived SEM micrographs of brass, aluminum and mild steel worn under synthetic oil and waste cooking oil lubrication, one specimen per condition, were analyzed with brightness-invariant texture descriptors and compared with the measured wear, friction and roughness. From the present study, it can be concluded that:

Worn aluminum surfaces in this archive are less directional (orientation order 0.71 against 0.96 and 0.91) and carry more high-contrast features (3.3% against 2.4% and 3.0%) than brass and mild steel, consistently across imaging voltages and processing parameters; the difference is large but, with 4 to 5 specimens per metal, not statistically established ($p = 0.09$), and its directional part is already present in the unworn finishing texture.

Mild steel at 80 °C under 50% WCO shows a strongly grooved surface (anisotropy 21 against 1.7 at 40 °C) that coincides with a roughly fifteen-fold rise in measured Ra relative to 22 °C and a near tripling of friction relative to 40 °C; this is a single-specimen observation that warrants replication.

Within each metal, replacing half the synthetic oil with waste cooking oil produced no difference in worn-surface texture approaching the size of the metal or temperature differences; the data are insufficient to establish or exclude a smaller effect, and pure WCO could not be compared at 40 N.

None of the 30 descriptor–response correlations across the 13 conditions is significant; single, operator-selected SEM fields document gross surface morphology but should not be used to rank lubricants or to infer wear rate. The descriptors respond to directionality and high-contrast features of any origin, including machining marks, and do not identify wear mechanisms by themselves; unworn references must be measured alongside worn surfaces.

https://doi.org/10.3390/lubricants14110435

Author Contributions: Conceptualization, A.E.A.; Methodology, A.E.A.; Software, A.E.A.; Writing—original draft, A.E.A., J.A. and B.F.Y.; Writing—review & editing, A.C.O., K.K., J.A. and B.F.Y.; Supervision, K.K. and B.F.Y. All authors have read and agreed to the published version of the manuscript.

Funding: This research received no external funding.

Data Availability Statement: The original contributions presented in this study are included in the article. Further inquiries can be directed to the corresponding authors.

Conflicts of Interest: The authors declare no conflict of interest.

References

1. Abdullah, M.I.H.C.; Abdollah, M.F.B.; Amiruddin, H.; Tamaldin, N.; Nuri, N.R.M. Optimization of tribological performance for filtration waste cooking oil enhance by ZrO_2 and graphite nanoparticle. In Proceedings of the Malaysian International Tribology Conference 2013, MITC20, Sabah, Malaysia, 18–20 November 2013; Volume 13, pp. 313–319. [CrossRef]
2. Alotaibi, J.G. Wear and Frictional Performance of Metals Under Dry/Waste Cooking Oil Lubricant Conditions. Ph.D. Thesis, University of Southern Queensland, Toowoomba, Australia, 2014.
3. Ayyadevara, S.N.; Das, P.; Sarker, M.I.; Sharma, B.K.; Roy, S. Analyzing the potential of waste cooking oils as biolubricants for electric vehicles. *RSC Adv.* **2026**, *16*, 12884–12901. [CrossRef] [PubMed]
4. Fasogbon, S.K.; Oyedepo, S.O. Nano-additive blends examination of performance and emission profile of CI engines fuelled with waste cooking oil based-biodiesel. *J. Therm. Eng.* **2025**, *11*, 1–15. [CrossRef]
5. Riayatsyah, T.M.I.; Sebayang, A.; Silitonga, A.; Benu, S.M.; Kalam, A.; Nurulita, B.; Sebayang, A.R.; Damanik, N.; Deswita; Zulkifli, N. Valorisation of non-edible and waste cooking oils into hybrid biolubricants: A tribological study. *Ind. Crops Prod.* **2026**, *240*, 122693. [CrossRef]
6. Alotaibi, J.G.; Yousif, B.F.; Yusaf, T.F. Brass, aluminium, and mild steel sliding against stainless steel under dry conditions. *Int. J. Precis. Technol.* **2015**, *5*, 85. [CrossRef]
7. Alotaibi, J.G.; Yousif, B.F.; Yusaf, T.F. Wear behaviour and mechanism of different metals sliding against stainless steel counterface. *Proc. Inst. Mech. Eng. Part J J. Eng. Tribol.* **2014**, *228*, 692–704. [CrossRef]
8. Hairunnaja, M.A.; Alazemi, A.A.; Aziz, M.A. From Waste to Lubrication Resource: A Systematic Review of Waste Cooking Oil-Based Greases and Liquid Lubricants. *Lubricants* **2026**, *14*, 260. [CrossRef]
9. Opia, A.C.; Bin Abdollah, M.F.; Mamah, S.C.; Hamid, M.A.; Syahrullail, S.; Amiruddin, H. Comparison on Tribological Responsiveness of Jatropha Lubricant Modified with H-BN on AISI E-52100 Steel and 6061 Aluminum Alloy Materials. In Proceedings of the Society of Petroleum Engineers—SPE Nigeria Annual International Conference and Exhibition, NAIC 2025, Lagos, Nigeria, 4–6 August 2025. [CrossRef]
10. Grabovic, E.; Damiano, R.; Irene, A.; Derobertis, F.; Leone, S.L.; Dell'Anna, M.M.; D'Accardi, E.; Mele, M.; Ciulli, E.; Seggiani, M. Rheological and tribological properties of waste cooking oil-derived bio-lubricants through multiple chemical routes. *Biomass Bioenergy* **2027**, *216*, 109649. [CrossRef]
11. Yang, H.; Li, Z.; Feng, C.; Pang, M. Tribological Performance of 304 Stainless Steel with Surface Texture Fabrication in $CuSO_4$ Liquid Using Laser Method. *J. Mater. Eng. Perform.* **2025**, *35*, 4900–4910. [CrossRef]
12. Bhaumik, S.; Paleu, V.; Chowdhury, D.; Batham, A.; Sehgal, U.; Bhattacharya, B.; Ghosh, C.; Datta, S. Tribological Investigation of Textured Surfaces in Starved Lubrication Conditions. *Materials* **2022**, *15*, 8445. [CrossRef] [PubMed]
13. Ma, C.; Duan, Y.; Yu, B.; Sun, J.; Tu, Q. The comprehensive effect of surface texture and roughness under hydrodynamic and mixed lubrication conditions. *Proc. Inst. Mech. Eng. Part J J. Eng. Tribol.* **2017**, *231*, 1307–1319. [CrossRef]
14. Xie, Z.; Li, J.; Tian, Y.; Du, P.; Zhao, B.; Xu, F. Theoretical and experimental study on influences of surface texture on lubrication performance of a novel bearing. *Tribol. Int.* **2024**, *193*, 109351. [CrossRef]
15. Shah, R.; Juran, B.; Nitodas, S. Eco-Friendly Production of Sustainable Bio-Based Lubricants with Green-Synthesized Nanoparticles. *Lubricants* **2026**, *14*, 327. [CrossRef]
16. Ou, Z.; Wu, W.; Dai, H. Quantitative analysis of grinding performance of cubic silicon carbide surface texture lubricated with water film. *Tribol. Int.* **2023**, *180*, 108267. [CrossRef]
17. Pawlus, P.; Reizer, R.; Wieczorowski, M. Parametric Characterization of Machined Textured Surfaces. *Materials* **2022**, *16*, 163. [CrossRef] [PubMed]
18. Antoszewski, B.; Kurp, P. Effect of Surface Texture on the Sliding Pair Lubrication Efficiency. *Lubricant* **2022**, *10*, 80. [CrossRef]
19. Yu, C.; Cheng, R.; Zhang, H.; Ma, C.; Yu, S. The Influences of Surface Texture Topography and Orientation on Point-Contact Mixed Lubrication. *Lubricants* **2025**, *13*, 409. [CrossRef]
20. Bigun, J.; Granlund, G.H.; Wiklund, J. Multidimensional orientation estimation with applications to texture analysis and optical flow. *IEEE Trans. Pattern Anal. Mach. Intell.* **1991**, *13*, 775–790. [CrossRef]

21. Jacobs, T.D.B.; Junge, T.; Pastewka, L. Quantitative characterization of surface topography using spectral analysis. *Surf. Topogr.* **2017**, *5*, 013001. [CrossRef]
22. Persson, B.N.J.; Albohr, O.; Tartaglino, U.; Volokitin, A.I.; Tosatti, E. On the nature of surface roughness with application to contact mechanics, sealing, rubberfriction and adhesion. *J. Phys. Condens. Matter* **2004**, *17*, R1. [CrossRef] [PubMed]
23. Opia, A.C.; Bin Abdollah, M.F.; Kadirgama, K.; Syahrullail, S.; Amiruddin, H.; Veza, I. Analysis on tribological performance and mechanisms of h-BN, MWCNTs, CuO and EC-CNTs nano additives in different lubricants. *Surf. Interfaces* **2026**, *87*, 108911. [CrossRef]
24. Zhang, Y.; Wang, B.; Cui, W.; Barber, G.C.; Hu, M. Assessment of tribological properties of oil-based flake WS_2-oleic acid lubricant on steel-brass sliding contact. *Tribol. Online* **2020**, *15*, 293–299. [CrossRef]
25. Rajkumar, K.; Vasudevan, S.; Subbiah, N. A Comparative Study on the Brass-Steel Tribo-Pair under Dry and Lubricated Sliding Conditions. *Appl. Mech. Mater.* **2016**, *852*, 416–421. [CrossRef]
26. Ajimotokan, H.A. Lubricants and Materials for Tribological Applications. In *Principles and Applications of Tribology*; Springer Nature: Cham, Switzerland, 2024; pp. 47–72. [CrossRef]
27. Decrozant-Triquenaux, J.; Pelcastre, L.; Prakash, B.; Hardell, J. Influence of lubrication, tool steel composition, and topography on the high temperature tribological behaviour of aluminium. *Friction* **2021**, *9*, 155–168. [CrossRef]
28. Zheng, K.; Dong, Y.; Dong, H.; Fernandez, J.; Dean, T.A. Investigation of the lubrication performance using WC: C coated tool surfaces for hot stamping AA6082. *Procedia Eng.* **2017**, *207*, 711–716. [CrossRef]
29. Schell, L.; Sellner, E.; Michael, M. Tribology in Warm and Hot Aluminum Sheet Forming—Transferability of Strip Drawing Tests to Forming Trials. *Adv. Eng. Mater.* **2023**, *23*, 107449. [CrossRef]
30. Ali, A.I.; Hamid, M.K.A.; Bin Abas, M.A.; Said, M.F.M.; Mazali, I.I.; Daud, Z.H.C.; Opia, A.C. Experimental analysis of tribological performance of base ficus carica vegetable oil with different polymers as additives using four ball tribometer. *Mater. Today Proc.* **2022**, *110*, 9–14. [CrossRef]
31. Xie, J.; Hu, S.; Liu, C.; Gao, Z.; Zhang, F.; Zhang, C.; Ali, M.K.A. Enhancing the Lubrication Performance of Steel–Steel Contacts Using a Novel Ionic Liquid Based on Phosphate Ammonium Salt as an Oil Additive. *Lubricants* **2026**, *14*, 21. [CrossRef]
32. Ali, A.I.; Hamid, M.K.A.; Abas, M.A.; Paiman, Z.; Said, M.F.M.; Opia, A.C.; Syahrulail, S.; Izmi, I.; Daud, Z.H.C. Assessment on oxidative stability and tribological response of Ficus carica Oil, enhanced with TBHQ and EVA additives. *Tribol. Int.* **2025**, *209*, 110735. [CrossRef]
33. Gangopadhyay, A.; Sinha, K.; Uy, D.; McWatt, D.G.; Zdrodowski, R.J.; Simko, S.J. Friction, wear, and surface film formation characteristics of diamond-like carbon thin coating in valvetrain application. *Tribol. Trans.* **2021**, *54*, 104–114. [CrossRef]
34. Wang, H.; Shao, Z.; Shen, K.; Bateer, B.; Ren, F.; Qi, X. Super Hydrophobic UHMWPE/PTFE/PVA Composites with Low Friction: Preparation and Wear Mechanism. *Polymers* **2025**, *17*, 1664. [CrossRef] [PubMed]
35. Celik, I.; Şensoy, A.T.; Seze, S.B. Evaluation of Lubricant Selection and Lubrication Intervals for Pin–Bushing Bearings Operating Under High-Temperature Conditions in Heavy-Duty Construction Machinery. *Lubricants* **2026**, *14*, 179. [CrossRef]
36. Zheng, A.L.T.; Teo, E.Y.L.; Marzuki, O.F.; Koo, L.F.; Wong, T.J.; Chung, T.L.T.; Andou, Y. Additive manufacturing of high-performance adsorbents for environmental use. *Eng. Res. Express* **2026**, *7*, 032001. [CrossRef]

Disclaimer/Publisher's Note: The statements, opinions and data contained in all publications are solely those of the individual author(s) and contributor(s) and not of MDPI and/or the editor(s). MDPI and/or the editor(s) disclaim responsibility for any injury to people or property resulting from any ideas, methods, instructions or products referred to in the content.